Materials Characterization 189 (2022) 111931

Contents lists available at ScienceDirect

Materials Characterization

journal homepage: www.elsevier.com/locate/matchar

High resolution crystal orientation mapping of ultrathin films in SEM and TEM

Mario F. Heinig [a,e], Dipanwita Chatterjee [b], Antonius T.J. van Helvoort [b], Jakob Birkedal Wagner [a], Shima Kadkhodazadeh [a], Håkon Wiik Ånes [c], Frank Niessen [d], Alice Bastos da Silva Fanta [a,*]

[a] DTU Nanolab, Technical University Denmark, DTU, Kgs. Lyngby, Denmark
[b] Department of Physics, Norwegian University of Science and Technology, NTNUTrondheim, Norway
[c] Department of Materials Science and Engineering, Norwegian University of Science and Technology, NTNU, Trondheim, Norway
[d] Department of Mechanical Engineering Materials and Surface Engineering, Technical University Denmark, DTU, kgs. Lyngby, Denmark
[e] Xnovo Technology ApS, Køge, Denmark

ARTICLE INFO

Keywords:
Microstructure
Ultrathin films
TKD
SPED
Immersion mode

ABSTRACT

Ultrathin metallic films are important functional materials for optical and microelectronic devices. Dedicated characterization with high spatial resolution and sufficient field of view is key to the understanding of the relation between microstructure and optical and electrical properties of such thin films. Here, we have applied on-axis transmission Kikuchi diffraction (TKD) and scanning precession electron diffraction (SPED) to study the microstructure of 10 nm thick polycrystalline gold films. The study compares the results obtained from the same specimen region by the two techniques and provides insights on the limits of each diffraction technique. We compare the physical spatial resolution of on-axis TKD and SPED and discuss challenges due to the larger probe size in scanning electron microscopy (SEM). Moreover, we present an improvement for the physical spatial resolution (PSR) of on-axis TKD through acquisition in immersion mode. We show how this method extends the capabilities of SEM-based microstructure characterization of ultrathin films and achieve PSR comparable to semi-automated SPED.

1. Introduction

Metallic thin films with 10 nm and below thicknesses are of interest for a number of applications, including electrochemical and optical sensors [1,2] and organic photovoltaics [3–5]. The macroscopic properties of these structures are largely influenced by their microstructure, and the effect of grain size, orientation, boundaries, and structural defects on optical and electrical properties have been demonstrated previously [6–11]. Consequently, the detection of fine grain structures and the characterization of such features are essential and an ongoing topic of research [12–14]. In this respect, automated crystal orientation mapping (ACOM) methods in an electron microscope are ideal, as they provide fast and spatially resolved crystal phase and orientation information. In addition, these enable the semi-automatic determination of grain size, grain boundary character and distribution, along with texture and phase composition. Today, there are two major techniques providing sufficient resolution to map crystal orientations of nanometer-sized crystalline thin films: Scanning (Precession) Electron Diffraction (S(*P*)ED) in the transmission electron microscope (TEM) and transmission Kikuchi diffraction (TKD) in the scanning electron microscope (SEM). SPED is a TEM based technique in which spot diffraction patterns are automatically recorded and indexed, while the fine probe size of the precessing electron beam rasters over the specimen. The precession creates stable quasi-kinematic like patterns that ease the indexing [15]. SPED combined with ACOM allows for generating phase and orientation maps with a spatial resolution down to 2 nm [15,16]. This diffraction-based technique offers a high spatial resolution; however the signal contains information about the entire electron-transparent specimen thickness. Overlapping grains in the beam direction, such as inclined grain boundaries, may complicate the precise local determination of the grain size and orientation [17,18]. Another approach is to index Kikuchi patterns in an automated fashion by TKD in the SEM. This method was

* Corresponding author.
E-mail address: alice.fanta@cen.dtu.dk (A.B. da Silva Fanta).

https://doi.org/10.1016/j.matchar.2022.111931
Received 4 October 2021; Received in revised form 21 April 2022; Accepted 22 April 2022
Available online 27 April 2022

introduced in 2012 by Keller and Geiss [19], further developed to an on-axis system by Fundenberger et al. [20] and has gained growing attention in material science to study nanocrystalline and ultrafine grain materials. The physical spatial resolution is in the order of 6–10 nm [21,22] and the relatively large capture angle of Kikuchi patterns in the SEM allows high orientation accuracy. Furthermore, since the majority of the Kikuchi signal comes from the exit surface of the sample [23–25], overlapping grains cause less challenges for pattern indexing. Nevertheless, overlapping signal from different crystals is still commonly observed at grain boundaries due to the larger probe size through the sample in the SEM.

In principle, both techniques provide similar crystallographic information, but differ in terms of electron beam energy, probe and diffraction signal (spot or Kikuchi patterns) [26]. Previous studies have reported TKD and SPED analysis of the same specimen to determine their efficacy [27–29]. Yet, most of these studies worked with off-axis TKD systems, which do not have the optimal resolution capacity compared to the on-axis TKD technique [22]. Moreover, these results analyze grains of several tens of nanometer in size, rather than exploring the resolution limitations of the two techniques. Lee et al. [24] and Jeong et al. [30] reported comparison studies of the SEM and TEM based grain mapping techniques using an on-axis TKD system, however the investigated films were more than 50 nm thick and contained overlapping grains, leading to indexing uncertainties.

In this study, we have employed SPED and TKD analysis of the same specimen regions to characterize the microstructure of ultrathin Au films for conductive and optical sensitive thin film applications and compared the orientation determination, mapping capabilities and resolution of the two techniques. The thickness of such films is ideal for such a comparative study, as it minimizes the impact of overlapping grains and the differences that can arise due to the diffraction volume in each technique. Moreover, to achieve continuous Au films with thicknesses in the range of 10 nm and below, an adhesion promoter is inevitable; otherwise, the metal tends to agglomerate into isolated clusters [31]. Such an adhesion layer significantly influences the film microstructure, reducing its grain size typically to the same range as the film thickness, challenging the spatial resolution of both techniques, in particular TKD [21,22]. Our study, therefore, facilitates a direct comparison of the structural analysis by these two techniques, and tests sample thickness limitations for Kikuchi diffraction [24]. In addition, we present a new approach for on-axis TKD analysis by immersing the sample in a magnetic field (immersion mode), and show that this approach improves and extends the physical spatial resolution of microstructural orientation mapping in SEM to values that are comparable to TEM. The physical spatial resolution (PSR) was previously introduced by Zaefferer et al. [32] and is related to the interaction volume from which the diffraction signal originates.

2. Materials and Methods

2.1. Thin film fabrication

The thin films were deposited on 20 nm thick amorphous SiO_2 windows of commercially available TEM grids (TEMwindows.com). The metallic adhesion layer Ti and the Au thin film were deposited by DC sputtering, while the organic adhesion promoter, (3-aminopropyl)-silatrane (APS), was deposited following an immersion process described by Heinig et al. [33] under a fumehood in a class 1000 cleanroom at constant temperature ($22^\circ \pm 2^\circ$) and humidity ($44\% \pm 2\%$) conditions. The thickness of the Ti and APS adhesion layers were approximately 1.0 nm and 0.8 nm, respectively, while the Au films were 10 nm thick. Previous cross-section characterization of these samples confirmed that the adhesion layers were amorphous [34].

2.2. Transmission Kikuchi Diffraction (TKD)

TKD data was acquired with an FEI Nova 600 NanoSEM using an e-Flash HD EBSD detector with an Optimus TKD detector head by Bruker Nano GmbH. The orientation maps were acquired with the Au-film facing away from the incoming beam and toward the detector beneath the sample [35]. The samples were plasma cleaned inside the SEM chamber prior to the experiments using an Evactron decontaminator (XEI Scientific) for 5 min. The data was processed using the Esprit 2.2 software provided by Bruker and MTEX, an open-source Matlab-based toolbox [36]. The microscope was operated at 30 kV electron acceleration voltage using an aperture size of 30 μm and a working distance of 5.5 mm, with a detector distance of 14.5 mm. For the TKD data acquired in immersion mode, the working distance was increased to 6.5 mm to meet the constraints in the distance of the sample to the microscope pole piece for immersion mode. Additional acquisition parameters are listed in Table 1. It should be noted that these datasets do not contain post acquisition data processing to supplement unindexed data points or generate additional data points by cleaning. The immersion lens in the SEM extends a magnetic field onto the sample in order to form a smaller probe size and improve the spatial resolution of non-magnetic samples [37]. This magnetic field, however, also affects the TKD signal and generates distorted Kikuchi patterns. The distortion in the patterns is corrected before the indexing through correlation with a reference pattern acquired under conventional conditions.

2.3. Scanning Precession Electron Diffraction (SPED)

The SPED mapping was carried out using a JEOL JEM 2100F transmission electron microscope and operated at 200 kV in nanobeam diffraction mode with a NanoMEGAS ASTAR system. The external Stingray camera recorded the PED patterns with 8-bit dynamical range. The geometry of the pattern acquisition results in distortion effects, which are corrected during the data processing by importing distortion correction for the used acquisition conditions in the Index software from NanoMEGAS. The software returns crystal phase and orientation identification by a template matching process [15]. The TEM probe diameter of 2 nm was measured on the sample under experimental conditions, here in nanobeam diffraction mode with a 10 μm condenser aperture (C1), an alpha setting of 4 and spot size of 1 nm. The full width at half maximum of the beam intensity profile as estimated for beam size (FWHM 2 nm) was recorded with a calibrated Gatan 2k Ultra Scan CCD camera. The SPED patterns were acquired with a probe convergence semi-angle of 1 mrad, a precession angle of 0.7°, a frequency of 100 Hz and a camera length of 20 cm. The sample was positioned in the microscope with the Au film facing the incoming beam (reversed to the direction used for the TKD experiments). Additional acquisition parameters are listed in Table 1.

2.4. Scanning Transmission Electron Microscopy (STEM)

Annular dark field scanning transmission electron microscopy (ADF STEM) images were recorded using an FEI Titan TEM instrument equipped with a spherical aberration correction unit on the probe-forming lenses and operated at 300 kV. The probe size and

Table 1
Summary of TKD and SPED acquisition parameters.

Parameter	On-axis TKD standard mode	SPED
Accelerating voltage [kV]	30	200
Beam current [nA]	1.7	0.200
Pattern resolution [pixels]	400 × 300	144 × 144
Exposure time [ms]	10.5	20
Step size [nm]	2	2
Acquisition time [min]	30	35
Indexing success rate [%]	~60–80	~80–90

convergence semi-angle used for the ADF STEM images were approximately 0.1 nm and 17 mrad, respectively, and the inner collection angle of the ADF images was 37 mrad. The images have 1024 × 1024 pixels and were recorded with a dwell time per pixel of 10 μs.

3. Results and Discussion

3.1. Comparison of SPED and TKD at the same position

Figs. 1 and 2 show inverse pole figure maps along the growth and beam direction (IPF-Z maps) of the Au/Ti/SiO_2 and Au/APS/SiO_2 samples, respectively, obtained using both TKD and SPED. The post-acquisition data processing is based on an averaged grain orientation, a grain definition, and a minimum grain size. The indexing thresholds of the measurements rest upon the reliability and resolution limits of the respective technique. Therefore, only data points with a minimum of 5 indexed Kikuchi lines or a reliability value of 5 for SPED are included. The reliability value is defined as the correlation indices for the first and second best solution of the template matching process, as stated by Viladot et al. [38] Manual comparison is done for prominent structural sample features (twins, triple points and grain boundaries) in correlation maps and STEM images. Furthermore, only grains with a pixel cluster (square grid pixel) larger than 4 in SPED and 8 in standard TKD are taken into consideration, consistent with the physical spatial resolution as shown later. The TKD maps from both samples contain noticeable areas, which could neither be indexed (less than 5 indexable Kikuchi bands), nor satisfy the predefined minimum grain size diameter and are represented by white regions in the maps of Fig. 1(a) and 2(a). No data cleaning was performed. The thin films, however, are continuous, as confirmed by secondary electron (SE) images and the fact that the unindexed regions still contain faint Kikuchi patterns (see supporting information (SI, Fig. S1)). Investigation of the same sample regions with SPED, (Fig. 1(b) and 2(b)) led to a reduction of the white, non-indexed areas. A few corresponding grains are labelled in the TKD and SPED maps for comparison. In both samples, the percentage of indexed pixels is increased from 80% to 90% for the Au/Ti/SiO_2 sample, and from 60% to 90% for the Au/APS/SiO_2 sample in the SPED data compared to TKD, and it becomes possible to resolve smaller grains (see Table 2). The SPED results in Fig. 2(d) suggest the preferential nucleation of ⟨001⟩ and ⟨101⟩ grains with sizes smaller than 10 nm in the APS sample, which could not be detected with TKD. It must be noted that the shown sample areas of the TKD orientation maps in Figs. 1(a) and 2(a) are selected regions from larger measured regions for illustration purposes (SI, Fig. S3). The histogram plots and indexing rate of the TKD maps in Figs. 1(c) and 2(c) are based on data from the entire scanned regions (SI, Fig. S3) to obtain better statistics and to partially compensate for the inevitable influence of contamination when investigating the same sample area. The TKD experiments were conducted after the SPED experiments, thus both the indexing rate and the pattern quality metric of the TKD maps may have been reduced in regions where the two maps overlap due to the beam induced specimen contamination. Consequently, the choice to not perfectly overlap the SPED and TKD experiments better accomodates for

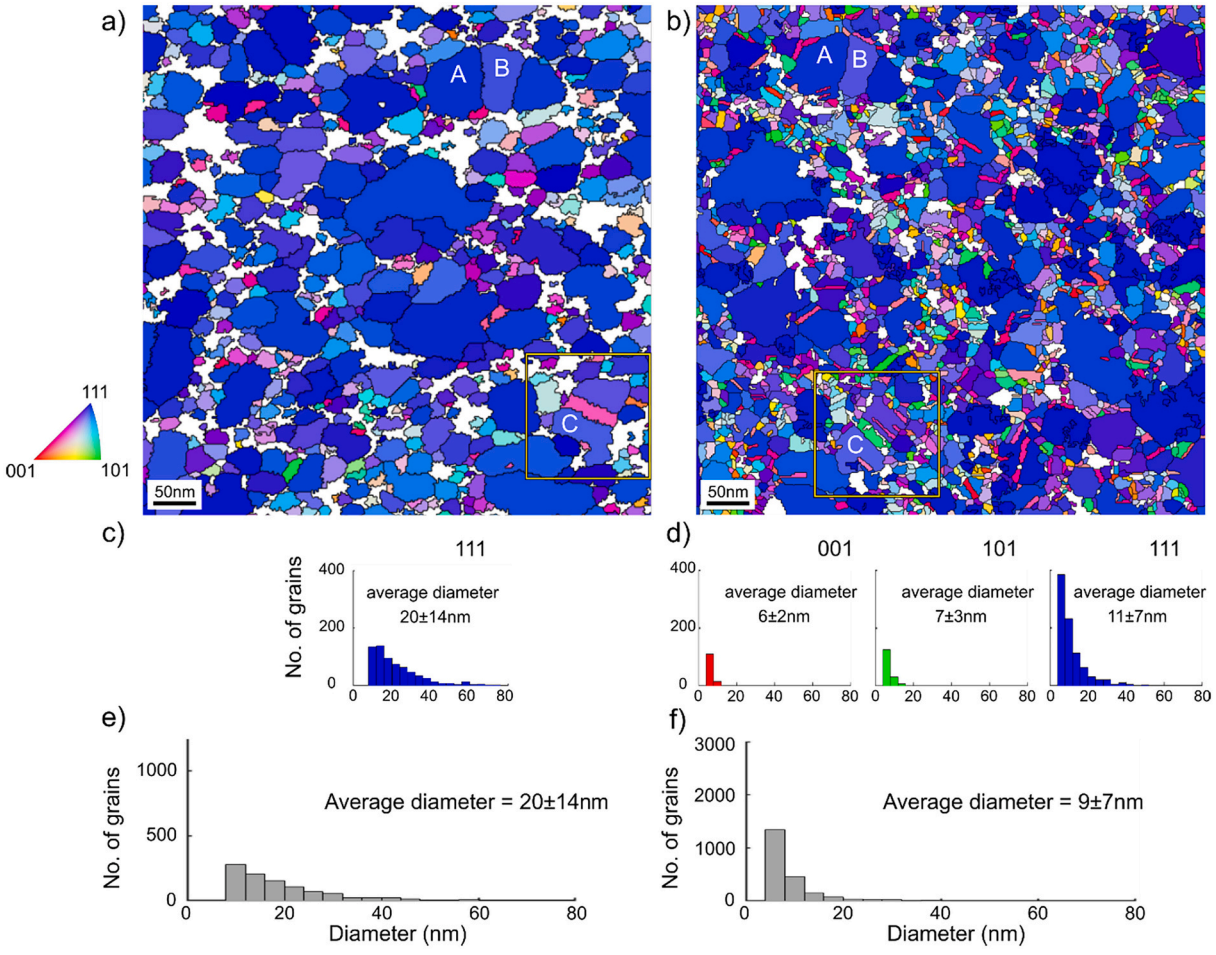

Fig. 1. IPF-Z maps of the Au/Ti/SiO_2 sample acquired by a) TKD standard mode, b) SPED, showing regions with identical grains, labelled A, B and C in both datasets. Figure c) and d) present histograms with size distributions of ⟨100⟩, ⟨101⟩ and ⟨111⟩ grains and e) and f) the total grain size distribution of each sample. Highlighted areas (yellow boxes) are discussed in more detail later (Fig. 3). The TKD detection of <100>, <101> grains in the Au/Ti/SiO_2 sample is insufficient to present comparable histograms. (For interpretation of the references to colour in this figure legend, the reader is referred to the web version of this article.)

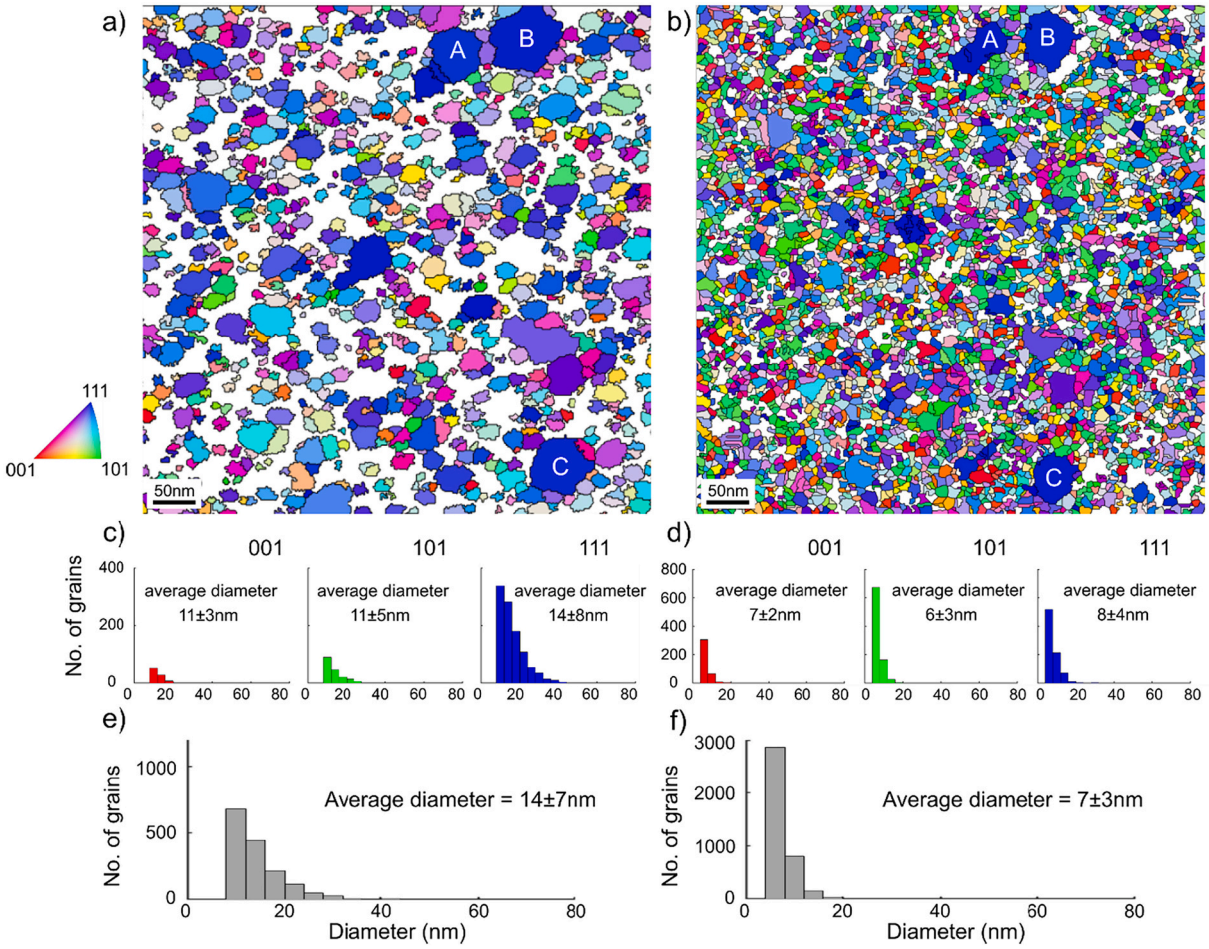

Fig. 2. IPF-Z maps of the Au/APS/SiO_2 sample acquired by a) TKD standard mode and b) SPED, showing regions with identical grains, labelled A, B and C in both datasets. Figure c) and d) present histograms with size distribution of the <100>, <101> and <111> grains and e) and f) the total grain size distribution of each sample.

Table 2
Mean grain size and standard deviation for both samples in standard mode TKD and SPED.

Sample	Standard mode TKD		SPED	
	Mean value [nm]	Std. dev. [nm]	Mean value [nm]	Std. dev. [nm]
Au/Ti/SiO_2	20	14	9	7
Au/APS/SiO_2	14	7	7	3

the evaluation of the contamination effects on the resolved microstructure (SI Fig. S3). For the Au/Ti/SiO_2 microstructure (Fig. S3a) a small improvement in indexing rate could be observed on the region only mapped with TKD. However, for Au/APS/SiO_2 microstructure, such improvement was not observed, indicating that specimen contamination was not the major factor contributing to the large fraction of unindexed points. In the future, it would be interesting to evaluate whether the order in which the measurements (TKD and SPED) are performed has an influence on the indexing rate and the resolved microstructure.

3.2. Highlighting some differences

Figs. 1 and 2 reveal significant differences in the mean grain size distribution between the orientation maps obtained by TKD and SPED and confirm the higher spatial resolution of SPED, which will be discussed later (Table 3). Furthermore, experimental factors such as drift and contamination, as well as induced beam damage due to repetitive measurements of the same sample regions also contribute to these differences.

In order to highlight some of the differences between the results obtained by TKD and SPED, a detailed analysis of the region around the labelled grain C of the Au/Ti/SiO_2 sample in Fig. 1 is presented in Fig. 3. This sample was chosen since its larger average grain size minimizes the effects of overlapping grains (SPED) and resolution limit (TKD). Nevertheless, we observe differences between the results from the two techniques. The ADF STEM image of the region in Fig. 3(a) was used as a reference. The IPF-Z maps from TKD and SPED of the region (Figs. 3(b) and (c)) show differences in terms of lateral spatial resolution (Fig. 3(d), (e)) and orientation indexing (Fig. 3(f), (g)). Fig. 3(b)–(e) clearly show that SPED can resolve smaller structural features, such as twins within the grain shown in Fig. 3(d) and (e), which is confirmed by the STEM ADF image. These twins are not resolved by the present TKD experiment (Fig. 3d). Even a careful investigation of the Kikuchi patterns within this grain does not reveal the presence of twins, indicating insufficient

Table 3
Physical spatial resolution calculated according to standard mode TKD and SPED.

	Standard mode TKD	SPED
Physical spatial resolution	8.7 ± 0.5 nm	5.2 ± 0.2 nm

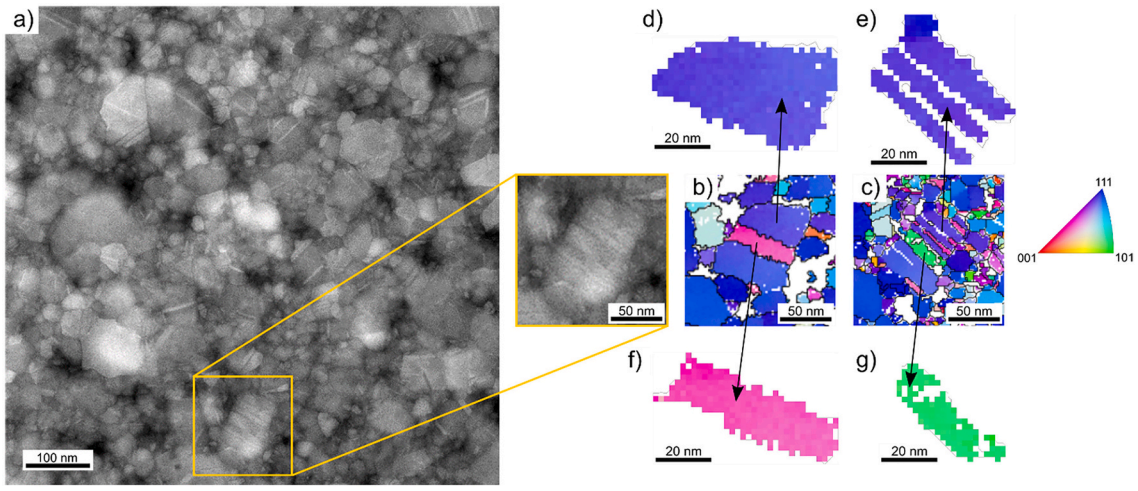

Fig. 3. STEM ADF image and IPF-Z maps of Au/Ti/SiO2 recorded by b) TKD standard mode and c) SPED. The selected area in a) STEM reference showing region with prominent grains d), e) high-lighting resolution (resolving twins) and indexing differences in SPED compared to f), g) in TKD. Grain labeled C in Fig. 1(a, b).

diffraction signal for Kikuchi diffraction analysis at 30 kV accelerating voltage from such small volumes. On the other hand, the grain highlighted in (f) and (g) points to misindexing of grains by the template matching process. Investigation of the raw diffraction patterns reveals a potential mismatch within the SPED map, due to the ambiguity of the patterns in <114> and <101> direction, resulting in a misindexed grain (see Fig. S2 in the SI). SPED is able to index the entire sample including nm-sized features, however the indexing software allocate a solution to every pixel and selects the most prominent diffraction pattern, which might not always represent the 3D sample configuration.

A careful comparison between the STEM ADF image and the SPED and TKD orientation map from another area within Fig. 3(a) is shown in the supporting information Fig. S6. The STEM images (Fig. 3 and S6) reveal small and dispersed areas (in the order of 20 nm) where the film thickness appears to be thinner than the rest of the film, and where the microstructure is finer. All grains indexed by TKD were also observed in the STEM images. The few unindexed areas are located on the regions where the film appears thinner (and the microstructure finer). Thus, lack of sufficient diffraction volume and lateral spatial resolution may be the major factor contributing to the absence of TKD data. However, in some of these areas, patterns are observed but not indexed, indicating that the indexing criteria (minimum 5 bands) also contributes to the lack of orientation information. By comparing the SPED data with the STEM images, it is possible to observe that some grains indexed in the orientation map are not visible in the STEM image (Fig. S6 a and c). A further inspection of the matching correlation index values (Fig. S6 d) reveals a worst matching between the recorded diffraction pattern and the generated template for these areas, indicating indexing weakness of this method. In general, direct comparison between the matching correlation index map with the STEM ADF image reveals very good agreement, showing that the doubtful indexed areas of the map are a result of correlation criteria chosen here (reliability value of 5) and the indexing procedure applied. It is evident that improvement in the indexing procedure and a better metric for quality of indexing are required.

These results emphasize the challenge of obtaining accurate microstructure and texture determination of ultrathin films containing many grains with sub-10 nm dimensions. First, both thickness and lateral grain dimensions in such films provide challenges for TKD, in terms of signal-to-noise detection (small volume for Kikuchi diffraction) and achievable lateral spatial resolution, pushing TKD analysis to its limits. Second, although SPED provides the necessary resolution to overcome these challenges, its indexing routine still can be improved. Currently, intense spots near the direct beam tend to be assigned higher weights in the automated template matching procedure, causing indexation errors such as the one shown in Fig. 3(g). New detectors with improved signal-to-noise ratio (SNR) and better dynamic range, combined with new methods to facilitate the indexing of spots further out in the reciprocal space, were recently demonstrated [39] as promising pathways to resolve such issues.

Previous studies have reported that the specimen thickness has a large effect on the TKD signal [25], both in terms of the intensity of the Kikuchi signal and of the background intensity. Liu et al. [25] discussed the influence of thermal diffuse scattering on the background intensity of the patterns and suggested a high background intensity in Kikuchi patterns from Au films thinner than 12 nm. Furthermore, it has also been suggested that the minimum thickness for Kikuchi scattering is on the order of one-fourth of the electron extinction distance [40], which means if the diffraction signal arises from grains smaller than 2.5 to 6 nm at 30 kV (Au samples), no Kikuchi diffraction signal would be detected and clearly indexed. Both limitations were observed in the microstructure study of the Au films presented in Figs. 1, 2 and 3. First, the sample thickness of 10 nm reduces the Kikuchi pattern contrast in comparison to background intensity, and in several regions of the thin films, the automated indexing routine was unable to identify at least 5 Kikuchi bands to provide crystal orientation. New approaches [41] to average the signal of neighboring points and enhance the signal-to-background intensity are possible methodologies to overcome insufficient indexing. Moreover, it is also evident that some microstructural features are smaller than the minimum thickness for Kikuchi scattering (e.g., width of twins in Fig. 3(d)), consequently these features are completely missed by the TKD technique and would only be resolved in the SEM with additional information from spot patterns.

3.3. *Spatial resolution*

The physical spatial resolution (PSR) differs from the effective spatial resolution. The latter describes the effectively achievable spatial resolution obtained after pattern indexing. Overlapping signals appear at the proximity of a grain boundary and by multiple grains within the thickness. To investigate the physical spatial resolution of the diffraction measurements we used the pattern recognition routine described by Niessen et al. [21] to determine the PSR of TKD according to Zaefferer et al. [32]. The PSR describes the first appearance of a Kikuchi pattern in a neighboring grain [21], which was extended here to apply also to spot patterns, as shown in Fig. 4. The PSR is determined in each case by analyzing linescans over well-defined high-angle grain boundaries (HAGB) to identify the appearance of neighboring patterns. The results of this analysis are listed in Table 3. Both diffraction experiments used a

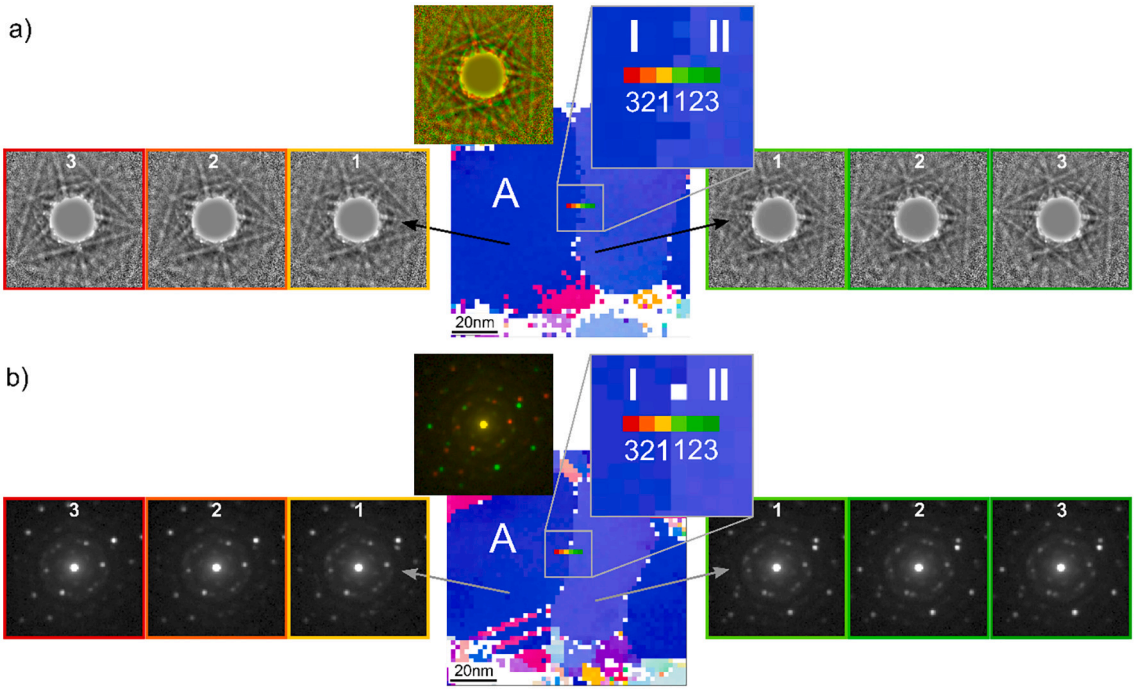

Fig. 4. Diffraction patterns recorded by a) standard mode TKD and b) SPED with a linescan (pattern position is colour-coded: "red-yellow-green") of the Au/Ti/SiO_2 sample across same HAGBs (misorientation >50°) to determine the PSR of both measurements. The linescan is applied at the grain boundary I-II of a selected grain, labelled 'A', and results in an overlap of two diffraction patterns visualized in green and red, in the center of a) and b) respectively. (For interpretation of the references to colour in this figure legend, the reader is referred to the web version of this article.)

2 nm step size, and the presented values are average PSRs over 5 HAGBs with their corresponding standard deviations (see Fig. S4 in SI for more details). The results in Table 3 are in-line with the qualitative observations of discrepancies between the average grain sizes measured by the two techniques, as TKD is unable to resolve many of the sub-10 nm grains present in the sample and thus, provides a spuriously larger average grain size. The smaller probe size in TEM naturally leads to the better PSR of SPED. It is important to point out that the PSR is also related to the depth from which the signal originates. Since spot patterns, in contrast to the Kikuchi patterns, originate from the entire sample thickness, the volume contributing to the diffraction signal in SPED can be larger than in TKD and overlapping signal from multiple grains within the thickness can influence the PSR results.

In this context it should be emphasized that orientation mapping also has an effective spatial resolution (ESR), which is defined by the ability of the indexing software to clearly distinguish between two overlapping patterns at a grain boundary (or within the PSR) [21]. The ESR is, in most of the cases, the spatial resolution provided in the literature [23,42] as it is the most significant for the resulting microstructure resolution. The ESR can be qualitatively estimated by investigating the number of non-indexed pixels at the grain boundaries. Although the PSR of on-axis TKD is inferior to SPED, for both techniques only a few single pixels at the grain boundaries are left un-indexed, leading to an ESR in the order of 2–4 nm for TKD and SPED, similar to the results previously presented in the literature [23,42]. On the other hand, the ESR significantly depends on the SNR of the patterns, the applied indexing routines and their set criteria. These effects play a significant role in the observed mean grain size differences in the orientation maps obtained by SPED and TKD (Figs. 1 and 2). The indexing system applied here on the Kikuchi patterns predefines a minimum of 5 Kikuchi bands for obtaining the crystal orientation of the pattern. The combination of weak diffraction signal (due to the sample thickness and current detector technology), fraction of overlapping patterns (due to a PSR relative to the grain size) and the set indexing pre-requisite hamper the orientation information from small grains. In addition, contamination and beam damage can reduce the SNR, which is a limiting factor for orientation indexing by means of TKD. In contrast, spot patterns used in SPED have a better SNR, and the indexing approach utilized for SPED orientation mapping is based on finding the best template matching solution. Subsequently, by careful evaluation, a reliability threshold is defined, and ambiguities and uncertainties are removed from the orientation map. Although both approaches allow orientation determination, the differences in the criteria and limiting characteristics make direct comparison less straight forward. Patterns from TKD with weak signals are difficult to index, particularly when these consist of overlapping diffraction signal from neighboring grains. On the other hand, as SPED data analysis always provides a solution, but not necessarily the correct one, it is therefore up to the user to evaluate the data and define its criteria. The reliability index scale is case dependent, and thresholding is subjective, and data set dependent. The example shown in Fig. 3(g) and S6(c) illustrates that even by careful definition of the reliability threshold (here done by comparing the STEM ADF images with the SPED data), misindexing can still occur. However, it should be noted that this anomaly is an exception as most grains indexed by TKD and SPED are in good agreement, which supports the choice of the reliability value of 5. Open-source initiatives such as used in Bergh et al. [43] like the pyXem software are under development to improve data evaluation and build more transparent analysis tools for diffraction datasets.

3.4. Improving TKD spatial resolution in immersion mode

The analysis above indicates, unsurprisingly, that the probe size is one of the experimental parameters affecting the physical spatial resolution of microstructural analysis. Moreover, a negligible amount of spread of the incoming electron beam over the 10 nm thin films for both TKD and SPED experiments is expected. With the aim of improving the PSR of the TKD orientation map, we performed a TKD investigation of the sample with the SEM in the immersion mode. In this mode, the magnetic field within the electron column of the microscope is extended, giving a finer probe. Fig. 5 presents TKD orientation maps of the same

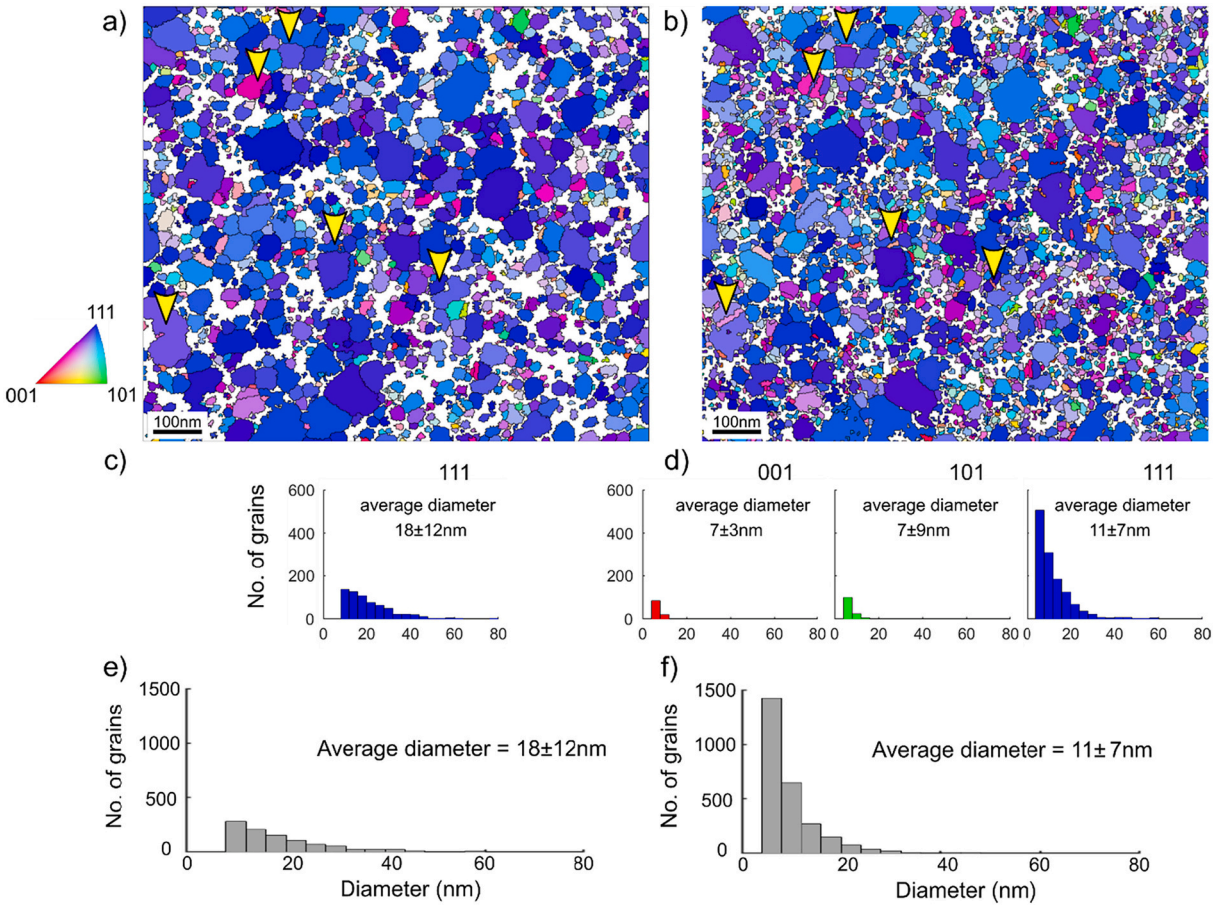

Fig. 5. IPF-Z maps acquired by TKD in a) standard mode and b) immersion mode of the same Au/Ti/SiO_2 sample area. Yellow arrows highlight the ability of the immersion mode to resolve fine structures, like twins in Figure b). The histograms in c), d) present the size distribution of the <100>, <101> and <111> grains and e), f) the total grain size distribution of the sample. The detection of <100>, <101> grains by the standard mode TKD is insufficient to present comparable histograms. (For interpretation of the references to colour in this figure legend, the reader is referred to the web version of this article.)

region of the Au/Ti/SiO_2 specimen performed in standard and immersion mode along with their respective grain size distribution histograms.

Comparison of the two maps in Fig. 5(a) and (b) clearly shows that the immersion mode can resolve and index smaller grains and details within the microstructure over the same field of view. As a result, finer microstructural features, such as twins (highlighted by arrows in Fig. 5) can be resolved with the immersion mode (Fig. 5(b)), similar to SPED analysis. The measured average grain size reduces from 18 ± 12 nm in standard mode to 11 ± 7 nm in immersion mode. Moreover, a larger number of <001> and <101> oriented grains are detected by the immersion mode compared to the standard mode (less than 50 grains), and as observed by the SPED texture analysis. Grains with these orientations tend to have smaller lateral dimensions [44] and are at the detection limit of standard TKD; however the limited number of <001> and <101> oriented grains are used as a qualitative analysis. The improved indexing rate in immersion mode is also reflected by the total number of indexed grains, which increases from ~1200 to over ~2800 applying the same data processing. Subsequently, a more accurate determination of the grain boundary fractions is achieved, as shown in Fig. S5. The PSR of the immersion mode is determined to be 5.4 ± 0.3 nm, following the same principle as before in Fig. 4, which shows a substantial improvement compared to the standard mode and is comparable to SPED (See Table 3).

The improved spatial resolution demonstrated by the TKD investigation in immersion mode is a promising step toward offering an adequate solution for nanocrystalline material characterization in the SEM. With this approach the PSR limitation of the SEM orientation technique is reduced, closing the gap between TKD and SPED for the analysis of nanocrystalline thin films. However, there is still a larger number of unindexed points in the orientation map (~15% unindexed). The reduction of the probe size in immersion mode should mostly affect the PSR, and only indirectly the ESR. This is because the ESR is strongly related to the indexing routine, but also dependent on the PSR, and overlapping patterns. Consequently, further improvements in respect to indexing routines are still required. Moreover, additional investigations to account for sample composition, thickness, and microscope parameters for immersion mode TKD are needed. Finally, it is expected that this advantage is limited to non-magnetic samples.

4. Conclusion

Electron microscopy techniques for crystal orientation mapping with nm-scale spatial resolution provide the best-suited platform to characterize ultrathin films. In this work, we demonstrate that the film thickness and lateral grain dimensions, pose challenges for conventional on-axis TKD in SEM. SPED in TEM has a higher spatial resolution and thereby a more complete characterization can be achieved. In fact, the ultrathin films minimize the risk of overlapping crystals, commonly affecting the accuracy of the spot pattern based automated crystal orientation determination and make our samples ideal for SPED. Both TKD and SPED reveal the microstructure and orientation of the ultrathin films, yet their physical spatial resolution (PSR of 8.7 nm vs 5.2 nm) and different orientation indexing methodologies lead to differences in grain size and orientation distributions. It is demonstrated that on-axis TKD in

immersion mode improves the PSR of TKD to 5.4 nm, which is close to that of SPED and enables the detection of fine microstructural features (e.g., nano-twins). This is a promising approach toward improving TKD characterization of ultrathin films with average grain size below 20 nm. While on-axis TKD only provides a solution if at least 5 Kikuchi bands are indexed by the automated routine, SPED always provides a solution, and thus, requires careful evaluation of the reliability criteria to ensure accurate microstructure description. Most of the very fine grains (< 10–15 nm) remain unresolved by TKD, due to either overlapping Kikuchi signal from adjacent grains or lack of sufficient signal from small crystal volumes. On the other hand, SPED can provide misleading finer grain sizes, due to indexing uncertainties. To further improve crystallographic description of sub-10 nm size microstructures it is essential to continue improving the indexing procedures of both techniques.

In general, the thinner the film, the more advantageous is SPED, as it is based on indexing spot patterns, which are available even for monolayer films. When sufficient thickness for the formation of Kikuchi patterns in the sample is available, TKD offers a good approach for accurate crystal orientation mapping, particularly considering angular resolution and the accessibility of the SEM-based techniques. However, if the microstructure is significantly finer than the film thickness, indexing ambiguities become a considerable challenge for SPED and sufficient diffraction volume from individual microstructure poses a challenge for TKD. Ultimately, combining both diffraction signals in a single technique would offer the best crystal orientation mapping solution for thin film characterization.

5. Data Availability

The raw and porecessed data require to reporduce these findings can be provided upon request.

Declaration of Competing Interest

The authors declare that they have no known competing financial interests or personal relationships that could have appeared to influence the work reported in this paper.

Acknowledgments

This project has received funding from the European Union's Horizon 2020 research and innovation programme under grant agreement No 823717 – ESTEEM3.

Appendix A. Supplementary data

Supplementary data to this article can be found online at https://doi.org/10.1016/j.matchar.2022.111931.

References

[1] M.B. Ali, F. Bessueille, J.M. Chovelon, A. Abdelghani, N. Jaffrezic-Renault, M. A. Maaref, C. Martelet, Use of ultra-thin organic silane films for the improvement of gold adhesion to the silicon dioxide wafers for (bio)sensor applications, Mater. Sci. Eng. C 28 (2008) 628–632.
[2] B.A. Sexton, B.N. Feltis, T.J. Davis, Characterisation of gold surface plasmon resonance sensor substrates, Sensors Actuators A Phys. 141 (2008) 471–475.
[3] J. Yun, Ultrathin metal films for transparent electrodes of flexible optoelectronic devices, Adv. Funct. Mater. 27 (2017).
[4] H.M. Stec, R.J. Williams, T.S. Jones, R.A. Hatton, Ultrathin transparent au electrodes for organic photovoltaics fabricated using a mixed mono-molecular nucleation layer, Adv. Funct. Mater. 21 (2011) 1709–1716.
[5] J. Zou, C.Z. Li, C.Y. Chang, H.L. Yip, A.K.Y. Jen, Interfacial engineering of ultrathin metal film transparent electrode for flexible organic photovoltaic cells, Adv. Mater. 26 (2014) 3618–3623.
[6] A. Kossoy, V. Merk, D. Simakov, K. Leosson, S. Kéna-Cohen, S.A. Maier, Optical and structural properties of ultra-thin gold films, Adv. Opt. Mater. 3 (2015) 71–77.
[7] J. Sotelo, J. Ederth, G. Niklasson, Optical properties of polycrystalline metallic films, Phys. Rev. B - Condens. Matter Mater. Phys. 67 (2003) 1–8.
[8] D.I. Yakubovsky, A.V. Arsenin, Y.V. Stebunov, D.Y. Fedyanin, V.S. Volkov, Optical constants and structural properties of thin gold films, Opt. Express 25 (2017) 25574.
[9] S.K. Pradhan, Observation of optical properties of gold thin films using spectroscopic ellipsometry, J. Mater. Sci. Eng. 05 (2016) 1–5.
[10] Q.G. Zhang, B.Y. Cao, X. Zhang, M. Fujii, K. Takahashi, Influence of grain boundary scattering on the electrical and thermal conductivities of polycrystalline gold nanofilms, Phys. Rev. B - Condens. Matter Mater. Phys. 74 (2006) 1–5.
[11] Y.F. Zhu, X.Y. Lang, W.T. Zheng, Q. Jiang, Electron scattering and electrical conductance in polycrystalline metallic films and wires: impact of grain boundary scattering related to melting point, ACS Nano 4 (2010) 3781–3788.
[12] G.S. Rohrer, Grain boundary energy anisotropy: a review, J. Mater. Sci. 46 (2011) 5881–5895.
[13] T. Watanabe, Grain boundary engineering: historical perspective and future prospects, Journal of Materials Science; Springer 46 (2011) 4095–4115.
[14] J. Xie, S. Li, R. Wang, H. Zhang, Y. Xie, Grain boundary engineering in atomically-thin nanosheets achieving bright white light emission, Chem. Sci. 5 (2014) 1328–1335.
[15] E.F. Rauch, M. Véron, Automated crystal orientation and phase mapping in TEM, Mater. Charact. 98 (2014) 1–9.
[16] I. Ghamarian, P. Samimi, Y. Liu, B. Poorganji, V.K. Vasudevan, P.C. Collins, Characterizing the nano-structure and defect structure of nano-scaled non-ferrous structural alloys, Mater. Charact. 113 (2016) 222–231.
[17] A. Valery, E.F. Rauch, L. ClÉment, F. Lorut, Retrieving overlapping crystals information from TEM nano-beam electron diffraction patterns, J. Microsc. 268 (2017) 208–218.
[18] B.H. Martineau, D.N. Johnstone, A.T.J. van Helvoort, P.A. Midgley, A.S. Eggeman, Unsupervised machine learning applied to scanning precession electron diffraction data, Adv. Struct. Chem. Imaging 5 (2019) 3.
[19] R.R. Keller, R.H. Geiss, Transmission EBSD from 10 nm domains in a scanning electron microscope, J. Microsc. 245 (2012) 245–251.
[20] J.J. Fundenberger, E. Bouzy, D. Goran, J. Guyon, H. Yuan, A. Morawiec, Orientation mapping by transmission-SEM with an on-axis detector, Ultramicroscopy 161 (2016) 17–22.
[21] F. Niessen, A. Burrows, A.B.S. da Fanta, A systematic comparison of on-axis and off-axis transmission Kikuchi diffraction, Ultramicroscopy 186 (2018) 158–170.
[22] Y. Shen, J. Xu, Y. Zhang, Y. Wang, J. Zhang, B. Yu, Y. Zeng, H. Miao, Spatial resolutions of on-axis and off-axis transmission Kikuchi diffraction methods, Appl. Sci. 9 (2019).
[23] G.C. Sneddon, P.W. Trimby, J.M. Cairney, Transmission Kikuchi diffraction in a scanning electron microscope: a review, Mater. Sci. Eng. R Reports 110 (2016) 1–12.
[24] S.Y. Lee, H.U. Guim, D.I. Kim, Y.C. Joo, C.H. Shim, J.P. Ahn, I.S. Choi, M. Abbasi, Transmission orientation imaging of copper thin films on polyimide substrates intended for flexible electronics, Scr. Mater. 138 (2017) 52–56.
[25] J. Liu, S. Lozano-Perez, A.J. Wilkinson, C.R.M. Grovenor, On the depth resolution of transmission Kikuchi diffraction (TKD) analysis, Ultramicroscopy 205 (2019) 5–12.
[26] J.D. Sugar, J.T. McKeown, D. Banga, J.R. Michael, Comparison of orientation mapping in SEM and TEM, Microsc. Microanal. 1–11 (2020).
[27] A. Garner, A. Gholinia, P. Frankel, M. Gass, I. Maclaren, M. Preuss, The microstructure and microtexture of zirconium oxide films studied by transmission electron backscatter diffraction and automated crystal orientation mapping with transmission electron microscopy, Acta Mater. 80 (2014) 159–171.
[28] M. Abbasi, D.-I. Kim, H.-U. Guim, M. Hosseini, H. Danesh-Manesh, M. Abbasi, Application of transmitted Kikuchi diffraction in studying nano-oxide and ultrafine metallic grains, ACS Nano 9 (2015) 10991–11002.
[29] R.G. Mariano, A. Yau, J.T. McKeown, M. Kumar, M.W. Kanan, Comparing scanning electron microscope and transmission electron microscope grain mapping techniques applied to well-defined and highly irregular nanoparticles, ACS Omega 5 (6) (2020) 2791–2799, acsomega.9b03505.
[30] J. Jeong, W.S. Jang, K.H. Kim, A. Kostka, G. Gu, Y.M. Kim, S.H. Oh, Crystallographic orientation analysis of nanocrystalline tungsten thin film using TEM precession electron diffraction and SEM transmission Kikuchi diffraction, Microsc. Microanal. 237–249 (2020).
[31] R.F. Voss, R.B. Laibowitz, E.I. Allessandrini, Fractal (scaling) clusters in thin gold films near the percolation threshold, Phys. Rev. Lett. 49 (1982) 1441–1444.
[32] S. Zaefferer, On the formation mechanisms, spatial resolution and intensity of backscatter Kikuchi patterns, Ultramicroscopy 107 (2007) 254–266.
[33] M.F. Heinig, B. Da Silva, A. Fanta, J.B. Wagner, S. Kadkhodazadeh, Aminopropylsilatrane linkers for easy and fast fabrication of high-quality 10 nm thick gold films on SiO2 substrates, ACS Appl. Nano Mater. 3 (2020) 4418–4427.
[34] M. Todeschini, Bastos Da Silva, A. Fanta, F. Jensen, J.B. Wagner, A. Han, Influence of Ti and Cr adhesion layers on ultrathin Au films, ACS Appl. Mater. Interfaces 9 (2017).
[35] K.P. Rice, R.R. Keller, M.P. Stoykovich, Specimen-thickness effects on transmission Kikuchi patterns in the scanning electron microscope, J. Microsc. 254 (2014) 129–136.
[36] F. Bachmann, R. Hielscher, H. Schaeben, Grain detection from 2d and 3d EBSD data-specification of the MTEX algorithm, Ultramicroscopy 111 (2011) 1720–1733.
[37] Q. Xing, Information or resolution: which is required from an SEM to study bulk inorganic materials? Scanning 38 (2016) 864–879.
[38] D. Viladot, M. Véron, M. Gemmi, F. Peiró, J. Portillo, S. Estradé, J. Mendoza, N. Llorca-Isern, S. Nicolopoulos, Orientation and phase mapping in the

transmission electron microscope using precession-assisted diffraction spot recognition: state-of-the-art results, J. Microsc. 252 (2013) 23–34.
[39] J. Jeong, N. Cautaerts, G. Dehm, C.H. Liebscher, Automated crystal orientation mapping by precession electron diffraction-assisted four-dimensional scanning transmission electron microscopy using a scintillator-based CMOS detector, Microsc. Microanal. 27 (2021) 1102–1112.
[40] A. Deal, T. Hooghan, A. Eades, Energy-filtered electron backscatter diffraction, Ultramicroscopy 108 (2008) 116–125.
[41] P.T. Brewick, S.I. Wright, D.J. Rowenhorst, NLPAR: non-local smoothing for enhanced EBSD pattern indexing, Ultramicroscopy 200 (2019) 50–61.
[42] P.W. Trimby, Orientation mapping of nanostructured materials using transmission Kikuchi diffraction in the scanning electron microscope, Ultramicroscopy 120 (2012) 16–24.
[43] T. Bergh, D.N. Johnstone, P. Crout, S. Høgås, P.A. Midgley, R. Holmestad, P. E. Vullum, A.T.J. van Helvoort, Nanocrystal segmentation in scanning precession electron diffraction data, J. Microsc. 279 (2020) 158–167.
[44] M. Todeschini, Bastos da Silva, A. Fanta, F. Jensen, J.B. Wagner, A. Han, Influence of Ti and Cr adhesion layers on ultrathin Au films, ACS Appl. Mater. Interfaces 9 (2017) 37374–37385.